Mathematical Biosciences and Engineering

MBE, 17(5): 4657–4677.
DOI: 10.3934/mbe.2020256
Received: 26 May 2020
Accepted: 01 July 2020
Published: 07 July 2020

http://www.aimspress.com/journal/MBE

Research article

The mechanism of resistance-reducing/anti-adhesion and its application on biomimetic disc furrow opener

Jiyu Sun [1], Yueming Wang [1], Shujun Zhang [2], Yunhai Ma [1], Jin Tong [1] and Zhijun Zhang [3,*]

[1] Key Laboratory of Bionic Engineering (Ministry of Education), Jilin University, Changchun, 130022, P. R. China
[2] School of Computing and Technology, Gloucestershire University, Cheltenham GL50 2HR, UK
[3] Key Laboratory of CNC Equipment Reliability (Ministry of Education) and School of Mechanical and Aerospace Engineering, Jilin University, Changchun, 130022, P. R. China

* **Correspondence:** Email: zhijunzhang@jlu.edu.cn; Tel: +86-431-85095760; Fax: +86-431-85095760-888.

Abstract: The black soil of Northeast China is sticky and agglomerates easily, which often adheres to the surface of a traditional furrow opener during the furrowing process. In this paper, biomimetic design principles in resistance-reducing, anti-adhesion and resistance-reducing mechanism of biomimetic disc furrow opener were studied. Nine kinds of singular convex hull, nine kinds of singular wedge and nine kinds of mixed convex hull and wedge structural biomimetic disc furrow opener were designed, and the furrowing process with the soil simulated by finite element method (FEM).Three types of biomimetic disc furrow opener with less resistance were manufactured by laser processing for comparative test in soil bin based on the simulation results. The test results showed that the resistance of the biomimetic disc furrow opener was less than that of the ordinary disc. The soil-disc stress, influence of biomimetic structures, moisture content and furrow speeds on resistance were discussed. The resistance-reducing rate of D-BC-3 reached the maximum value 15.36% at the furrow speed of 0.6 m/s and the soil moisture content of 20%. It is believed that the biomimetic design principles can provide the significant inspirations for the future design of disc furrow opener with drag reduction.

Keywords: biomimetic; disc furrow opener; resistance-reducing; optimal design

1. Introduction

The furrow opener plays a significant role in seeding as one of the most important parts of a planter. The furrow opener digs a furrow in accordance with agronomic requirements. While the seed and fertilizer are guided into the furrow, they are covered with wet soil. The process affects the operational effectiveness of the planter directly [1]. No-tillage is a method of annual planting without disturbing the soil through tillage while allowing the surface to be covered with crop residues and weeds. The seeding environment of a no-tillage planter differs from that of conventional tiller because the planter confronts a substantial amount of residue and hard soil. Therefore, the furrow opener of no-tillage planter requires the following characteristics compared with a traditional planter: (1) a sharp cutting edge is fundamentally required to reduce resistance and enhance the planter's ability to cut through residue and weeds. (2) In order to reduce clogging by residue and weeds, the tiller should possess anti-clogging characteristics. (3) The furrowing should not disturb the soil and possess a backfilling function, which helps to prevent the evaporation of water [2].

Recently, researchers have studied the structure, performance and other aspects of the planter furrow opener based on no-tillage conditions. The studies found that the inverted T-shaped chisel furrow opener has a better seed emergence rate (57%) than that of traditional furrow opener (32.1%) with a lager tillage resistance [3]. However, this kind of furrow opener requires big thrust force to cut into the soil and it is difficult to apply fertilizer at the same time. The hoe-type furrow opener performs better in relatively dry and hard geologic soil [4], while its working depth is unstable and with high energy consumptions. When a hoe-type furrow opener, double disc furrow opener and single disc furrow opener are used in sandy loam soil with a moisture content of 18.04%, the single disc furrow opener displays the best consistency of tillage depth, and the sowing spacing of the double disc furrow opener is the closest to a theoretical value [5]. The furrow opener with an arc-shaped cutting edge has a less soil disturbance and can create an excellent passage with the corn stubble cutting efficiency of 88.6% [6]. The maize stalk residue cutting is effective at all forward speeds with a double disc furrow opener with a plain rolling coulter which is best suited for energy-efficient agriculture [2].The groove furrowed by the rotary cutter disc is looser, and the soil disturbance is larger with higher energy consumption [7]. There are various kinds of furrow openers, however the existing ones have greater resistance and are prone to blockage when soil moisture is too high.

The finite element method (FEM) has been widely used to design tillage tools and to investigate the interaction between soil and tillage implements [8]. An incremental method is used to address the soil material nonlinear problem, and the trapezoidal method is used to solve the dynamic response in the furrowing process. The experimental results reveal that the relative error between analysis results and soil test results is 0.9%–9.0%, which could provide a reference for furrow opener design [9]. The FEM model of interaction between the moldboard and the soil (i.e., the Mohr-Coulomb model) has been established to study the influence of plow body angles on the draft force [10]. The relationship of traction resistance with forward speed and furrowing depth is linear. For every furrowing depth increase of 1 cm, furrow resistance increases 20% [11]. Based on the analysis of the interaction between the disc furrow opener and the soil, a mechanical model including disc parameters and soil characteristics has been constructed to accurately predict lateral and vertical forces. However, it has been found that it is relatively difficult to use the model to predict the traction force [12,13]. The structure and stress characteristics of the single planter furrow opener have been analyzed. A mathematic regression model of traction resistance and a mathematical model of the depth stability of a single planter furrow opener have been constructed. These models reveal stability factors of soil hardness between 16×10^5 Pa and 26×10^5 Pa, furrow opener penetration resistance between 689 N

and 980 N and traction resistance between 441 N and 784 N. Penetration and traction resistance increase with the increase in speed and counterweight [14]. By analyzing a prediction model for 12 types of disc furrow opener component actions, it has been found that the empirical model can be used to predict power consumption during the furrowing process. However, the model parameters do not include soil parameters. Although these models are based on assumptions, the differences in model accuracy reflect the practical significance of those assumptions, and the sliding force on the disc has a substantial impact on the force of the disc [15].

Certain animals that live in moist soil have evolved a special geometric structure that resists soil adhesion. Through long-term natural selection, these animals exhibit an ability to move highly efficiently in the soil with low energy consumption. Soil rarely adheres to them in a manner that would restrict freedom of movement [16]. Inspired by the surface structure of the dung beetle, a biomimetic sharp corner furrow opener was designed using biomimetic principles. With this biomimetic furrow opener, the furrow resistance is 14% lower than that of an ordinary sharp corner furrow opener [16]. The non-smooth body surface structure effectively reduces the area subject to soil adhesion and limits water film continuity. The surface reduces resistance due to the improved interfacial lubrication [17]. The surface of dung beetles head is a non-smooth structure consisting of protrusion and pits, which could effectively reduce the resistance and adhesion between the dung beetle and the soil [18]. Pangolin has digging habitation in moist place with a strong ability to burrow [19]. The whole body except abdomen is covered with keratin tile-shape scales which have a certain curvature change. These scales show a good wear resistance which not only protects the body against the damage of soil and sand during digging, but also has a supplementary role in digging process. In long-term natural selection, the head of dung beetle and the back of pangolin have formed the excellent body surface structure to suit the movement in the soil and limit water film continuity, which improves the interfacial lubrication to reduce resistance.

In this paper, biomimetic design principles and resistance-reducing mechanism of disc biomimetic furrow opener was investigated for reducing effect of furrowing resistance and soil adhesion on energy consumption. Based on the biomimetic design principles, biomimetic resistance-reducing disc furrow opener for conservation agriculture in Northeast China were designed and simulated by FEM. In following, verification tests were performed in the soil bin, the soil-disc stress, influence of biomimetic structures, moisture content and furrow speeds on resistance were discussed.

2. Materials and method

2.1. Biomimetic design principles in resistance-reducing, anti-adhesion

Between biology and engineering, there is a gap that needs biomimetic to connect each other. Biomimetic is not only simple copy from nature, and it extracts features or parameters from biology and sets those as biomimetic elements. Results can be used in engineering applications by redesign and simulation. The following are few principles in biomimetic design of resistance-reducing and anti-adhesion.

1) The biomimetic elements selection should consider the function or action of biological prototype that is close to the design object.

2) The biomimetic elements should be extracted geometry size and simple structures which is easy to design [20–26].

3) The kinds and combination of biomimetic elements should be considered, such as singular or multiple biomimetic elements, mixed or parallel arrangements.

4) The less surface roughness, the larger the absorption loads, which will result in the least resistance in the furrowing process. The less surface roughness should be considered as one of the design objects.

5) Simulation will be helpful to optimize the design, which not only saves time and money, also can improve design.

6) In addition to structures, the materials also should be considered in biomimetic design. The surfaces of some biology are low surface energy materials, which lead to resistance-reduced and anti-adhesion.

2.2. Resistance-reducing mechanism of biomimetic disc furrow opener

In fact, the soil is composed of soil particle, water, and air. The saturated soil is composed of soil particles and water. At tool-soil interface water particles forms a lubricating layer thus reducing friction between metal surface and soil. That is, the direct contact between the soil particles and opener surface is the water interface. The soil friction is mainly composed of internal friction and external friction [27]. The internal friction is generated by the relative sliding or rolling of soil particles or adjacent soil layers, which is related to the soil cohesion and internal friction angle [28]. The external friction is caused by the relative motion between the soil particles and external object, which corresponds to Coulomb law [29]. The external friction (F_e) is connected with soil moisture content, external object surface, and interface state. Its magnitude is relevant to the friction resistance caused by the positive pressure N and soil adhesion C_a, as shown in Eq. (1) [30],

$$F_e = N\tan\lambda + C_a A \tag{1}$$

where A - the projection area of the contact surface in the direction of vertical movement, λ - the friction angle between soil and external object. Obviously, the soil adhesion is the principal factor of external friction.

During metal-soil contact, the contact area is composed of five layers, metal layer, interface between metal surface and water film, water film, interface between water film and soil, soil layer [31], as shown in Figure 1. The adhesion is determined by the weakest layer in the five layers. According to Young equation, solid surface free energy E_s is related with water surface free energy E_w and metal-water interface free energy $E_{m\text{-}w}$ [32], as shown in Eq. (2).

$$E_s = E_w\cos\theta + E_{m-w} \tag{2}$$

Where θ - contact angle between water and metal surface.

Therefore, the adhesion W_a required to separate the interface between metal and water per unit shows in Eq. (3) [32].

$$W_a = E_s + E_w - E_{m-w} = E_w(1+\cos\theta) \tag{3}$$

Considering vapor layer absorbed in the solid surface producing dilatation pressure p, the actual $E_{m\text{-}s}$ should minus p. Therefore, actual adhesion work W_a' should be expressed in Eq. (4).

$$W_a' = E_w(1+\cos\theta) - p < W_a \tag{4}$$

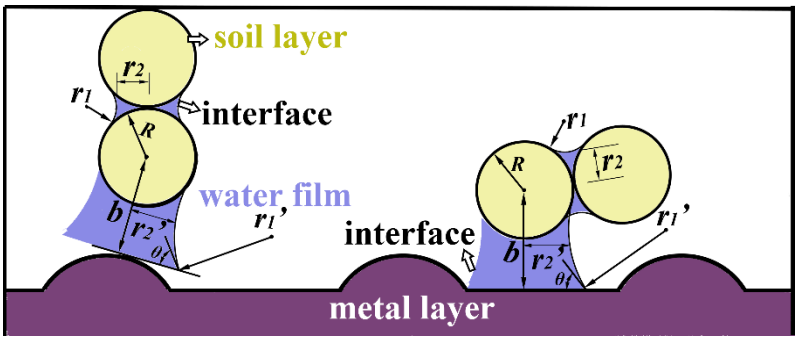

Figure 1. Five layers interface modeling.

The above analysis shows that the fracture layer will only occur in water film layer. Metal surface free energy, soil surface free energy, and water surface tension determine the adhesion work between metal and soil. The separation between metal and soil requires overcoming the attraction caused by water film, which depends on water film meniscus [33].

The soil adhesion is related to interface water film tension. Figure 1 shows that the contact point between two sphere soil particles with radius R forms water ring with double lens shape under certain moisture content to hold the soil together tightly. According to Fisher theory, the water film tension between soil particles $F_{s\text{-}s}$ is shown in Eq. (5) [34].

$$F_{s-s} = \pi r_2^2 \Delta F + 2\pi r_2 F_w \tag{5}$$

Where r_2 - the radius of the most concave part of water ring, ΔF - capillary pressure, $\Delta F = F_w(\frac{1}{r_1} - \frac{1}{r_2})$, r_1 - the water ring generatrix radius of curvature, F_w - water surface tension.

Therefore, $F_{s\text{-}s}$ can be simplified as follows,

$$F_{s-s} = \pi r_2 F_w(\frac{r_1 + r_2}{r_1}) \tag{6}$$

There are two kinds of adhesion between soil and metal, discontinuous water ring and continuous water ring. Under the transition from a discontinuous state to a continuous state, Nichols [35] puts forward that the water film tension between metal and soil $F_{m\text{-}s}$ $F_{m\text{-}s}$ is related with water film thickness, as shown in Eq. (7).

$$F_{m-s} = K 4\pi R F_w \cos\theta / b \tag{7}$$

where K -constant, θ_w - the surface contact angle, b - water film thickness.

Therefore, adhesion caused by single water film $F_{s\text{-}a}$ is shown in Eq. (8).

$$F_{s-a} = F_{s-s} + F_{m-s} \tag{8}$$

Water film state, such as thickness, area, and distribution, plays a major role in soil-metal adhesion. In addition, the water film depends on the contact point state between soil and metal, such as area, shape, distribution (contact point continuity and uniformity) [36]. Changing the metal surface structures can cause a change in the water film structure between soil and metal interface in this area.

The surface of soil animal is not smooth with a certain gap between the surface and soil, which effectively reduces the negative pressure of atmosphere on the soil and the attraction of animal surface to the soil [37]. The non-smooth surface is easy to form a number of small soil-free area, or water film discontinuous area, which reduce the actual contact area to lower adhesion [38]. In addition, the air film exists on the interface between the surfaces of soil animal and soil, can reduce friction and adhesion.

The disc cutting edge of the disc opener first cuts the soil during the furrow process, and then pushes the soil away from its surface to form a groove. In this process, its surface is squeezed and rubbed by soil which is similar to the dung beetle and pangolin digging. In this paper, the micro convexity structure of the dung beetle's pronotum and the protruding structure of the wedge in pangolin's dorsal scales abstracted as a coupling element was applied on the disc furrow opener. In addition, because of the laminated structure of clay soil, the soil is constantly affected by the convex component to easily form an area without soil in the biomimetic area when the soil moves on the surface of the biomimetic disc furrow opener [39]. The real contact area between the soil and the biomimetic disc furrow opener is not as large as that of the ordinary disc furrow opener. Therefore, F_e is also smaller according to Eq. (1).

However, the biomimetic elements on a disc furrow opener could be singular or coupling (Figure 2). Firstly, the parameters of biomimetic elements should be considered are the height of the convex hull h_1, the dimension of the convex hull D, the wedge height h_2, the wedge width h_3 and the wedge length L'. Also, the layout of those biomimetic elements should be considered, such as the biomimetic element spacing between different rings S_1, the biomimetic element angle with a ring δ.

2.3. Biomimetic disc furrow opener design

2.3.1. Biomimetic structural parameters

According to the previously summarized literature and the analysis of the biomimetic structures [16,17,23], the selected parameters and their sample values were as follows: the diameters of convex hull were D = 6 mm, 10 mm and 14 mm, the heights of the convex hull were h_1 = 1 mm, 3 mm and 4 mm, the height of the wedge was h_2 = 3 mm, the lengths were L' = 6 mm, 10 mm and 14 mm, and the width was h_3 = 6 mm.

2.3.2. Biomimetic disc furrow opener models

The model of an ordinary disc with the diameter of 300 mm (Figure 2; Disc10) was established by SolidWorks. The disc working drift angle of 5.75° and the working inclination angle of 10.21° were set up. Biomimetic convex hull structure disc (D-BCH), biomimetic wedge structure disc (D-BW) and biomimetic coupled structure disc with convex hull and wedge (D-BC) were performed on the ordinary

disc by laser processing. The following factors should be considered: h_1, D, h_2, the biomimetic element spacing between different rings S_1 = 2 mm, 4 mm and 6 mm, the biomimetic element angle with a ring δ = 7.2°, 9° and 12°, the distance from the outermost biomimetic unit to the edge of the disc of S_2 = 5 mm, and the layer number of the ring coupling element n = 3. An orthogonal test design was adopted to optimize the size of the coupling structure quickly and efficiently [17]. Nine groups of biomimetic models were constructed according to L(3^4) orthogonal experimental table (Figure 2).

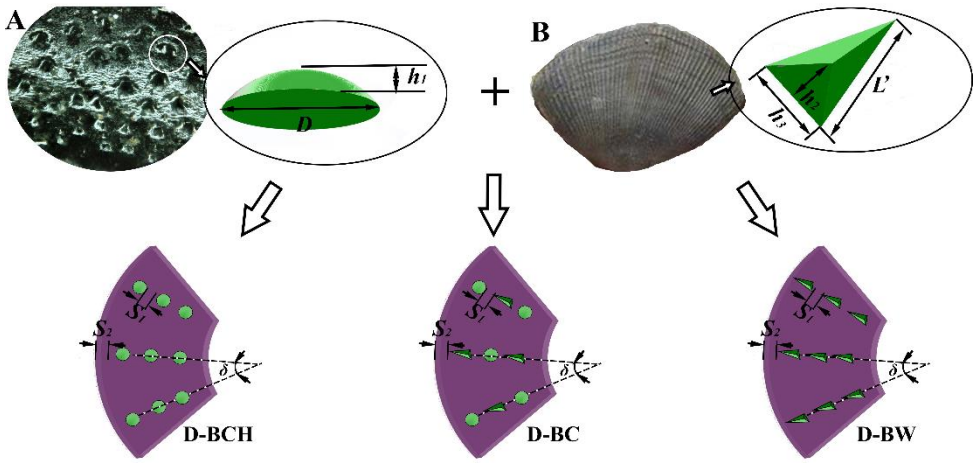

No.	1	2	3	4	5	6	7	8	9	10
h_1	1	1	1	3	3	3	4	4	4	
D/L'	6	10	14	6	10	14	6	10	14	
S_1	2	4	6	4	6	2	6	4	2	
δ	12°	9°	7.2°	7.2°	12°	9°	9°	7.2°	12°	Ordinary disc

Figure 2. Two types of biomimetic structural elements learn from dung beetle and pangolin. A, the micro convex hull structure of dung beetle pronotum; B, the wedge in pangolin's dorsal scale [23].

2.4. Biomimetic disc furrow opener design

2.4.1. Soil model

The quality of the simulation analysis mesh generation directly affects the computing time and the simulation accuracy. The soil model was a regular hexahedron. The mesh shape and size will affect calculation accuracy and simulation time. Therefore, the mesh with the same shape can be divided into regular hexahedrons, and the length of each mesh is 0.0008 m to balance the accuracy and calculation time. The finite element mesh is divided by the sweeping method with the number of 14282.

Table 1. Main material properties of soil used in the FEM simulation.

Property	Value
Soil particle density, RO (kg/m³)	2.08×10^3

Drawing selection of soil model information, NPLOT (Pa)	1
Specific gravity of soil used to obtain porosity, SPGRAV	2.68
Density of water in model units, RHOWAT (kg/m³)	1.00×10^{3}
Viscous parameter, VN	1.1
Viscoplasticity parameter, GAMMAR	0
Maximum number of plasticity iterations, ITERMAX	10
Initial bulk modulus or nonporous bulk modulus, k (Pa)	3.50×10^{7}
Shear modulus, G (Pa)	2.00×10^{7}
Internal friction angle, PHIMAX (°)	0.436
Level of damage that causes element deletion, DAMLEV (%)	0.9
Modified DO yield surface coefficient, AHYP	2.36×10^{3}
Cohesive force (Pa)	2.20×10^{4}
Eccentricity parameter for third invariant effects, ECCEN	0.7
Volumetric strain at initial damage threshold, DINT	2.50×10^{-3}
Strain hardening percent of peak shear strength angle, AN	0
Strain hardening amount of nonlinear effects, ET	0
Void formation energy, VDFM (J)	5.00×10^{-3}
Moisture content, MCONT (%)	18
Parameter for pore-water effects on bulk modulus, PWD1	0
Skeleton bulk modulus, pore-water parameter, PWKSK	0
Parameter for pore-water effects on effective pressure, PWD2	0
Minimum internal friction angle (radians), PHIRES (°)	0
Minimum internal friction angle (radians)	0
Maximum principal failure strain, EPSMAX	0.7

Table 2. Material characteristics of ordinary and biomimetic opener discs.

Elastic modulus/Pa	Density/kg·m^{-3}	Poisson ratio
3.0×10^{11}	7800	0.3

2.4.2. Boundary conditions and loading

Since the model is geometrically and physically symmetric, only one half of the soil and disc opener models were simulated to save computing time. The dynamic load was added to the biomimetic disc furrow opener along the X forward direction with the speed of 1 m/s. The biomimetic disc was completely constrained in all directions except the X direction. Each node of the soil model was completely constrained in all faces except the top face and the face of the first contact with the disc. The non-reflecting boundary was set up on these four faces.

2.5. Soil bin tests

2.5.1. Testing site

Soil bin test was carried out at College of Biological and Agricultural Engineering, Jilin University. The soil bin (30 m long, 3 m wide and 0.8 m deep) was filled with the black soil, the mainly cultivated land soil in Northeast China, as shown in Figure 3A. Testing region was 20 m long. According to speed instability in the test vehicle starting and stopping, each test region was divided into 3 sections, and the middle section (12 m) was the test stability region for data acquisition.

2.5.2. Testing facility

The traction equipment for the furrow test of disc opener was the soil bin test vehicle with computer monitoring and auxiliary test designed and manufactured by Harbin Bona Science and Technology Co., Ltd. The power of traction equipment is 20 kW and the motion speed can be up to 7km/h. Planter was fixed on the mounting bracket, and the three hanging points on the mounting bracket was used to install sensors connected to three-point suspension of the test vehicle (Figure 3B). The data processing system collects the data by the sensor built-in the test vehicle and during furrow resistance test.

Figure 3. (A) Soil bin and (B) experimental device.

2.5.3. Soil conditions

The mechanical structure of the black soil used in the soil bin was good and its constitutive property was uniform. It was easy to smooth and recover the soil after each test.

Low soil moisture content was unfavorable for seed germination, and the soil moisture suitable for soybean sowing is 18%–20% in Northeast China. Higher soil moisture would lead to soil adhesion to the furrow opener, which seriously increased furrow resistance and energy consumption [16]. With years of drought in Northeast China, the soil moisture was less than 15%. To investigate the resistance-reducing performance under different soil moisture contents, two levels of soil moisture (15% and 20%) were selected. The appropriate soil moisture was maintained by using a field scout TDR 300

soil moisture meter (Spectrum Technologies, Inc., Painfield, IL).

The soil firmness at 50 mm and 70 mm soil depth was measured respectively with eight measuring points selected randomly in the soil bin by soil solidity meter. The measuring rod with a conical probe was slowly pressed vertically into the soil and the value was displayed until the probe reaching the depth of measurement. The soil firmness was shown in Table 3.

Table 3. Soil compactness in the test soil bin (kPa).

Depth(mm) \ Number	1	2	3	4	5	6	7	8	average
50	248	274	278	257	269	249	270	255	262.5
70	280	261	310	287	296	305	301	289	291.1

Before the furrow test, the soil should be processed with rotary tillage, soil compaction and water spray to meet the test requirement of the soil moisture content and soil firmness. Similarly, the soil texture should be uniform to ensure that the variable data of each test is accurate, and the test condition is consistent. The soil treatment was done 8 days before the start of the test.

2.5.4. Soil conditions

The furrow speed in soybean field is about 2–7 km/h (0.56–1.94 m/s) in Northeast China. In order to ensure stable and reliable test data and investigate the effect of furrow speed on resistance, the soil bin test vehicle travels speed at 0.6, 1.0 and 1.4 m/s safely and smoothly, which span the main the real furrow speed.

According to agronomic parameters, the suitable sowing depth of soy bean is 40-70mm. The soil moisture content and the furrow speed are chosen as variables. The furrow depth was 70 mm. The test scheme for the resistance of disc opener is shown in Table 4. The comprehensive test was divided into 24 groups, and each group was repeated 3 times to improve the measurement accuracy.

Table 4. Test scheme of furrow resistance.

level \ factor	Disc type	Furrow speed (m/s)	Soil moisture content (%)
1	biomimetic type	0.6	18
2	Ordinary type	1	22
3		1.4	

3. Results

3.1. FEM analysis

During the soil-disc interaction, Figure 4 shows a typical relationship for resistance versus displacement with different soil conditions. The soil starts as elastic (*OA* range) with all the bonding forces active, all the soil elements connects with each other. The soil enters the plastic deformation

when it reaches to point *A*. Then, the soil goes into inelastic phase until deformation in point *K* measured as strain component ε_x (in the direction of the disc's motion) reaching a predefined magnitude of ε_c [41], this process corresponds to point M_1. The bonding force in the first node is deactivated that leads a drop in the resistance. This process corresponds to point N_1. Then first the yielding condition is reached and next the instant when ε_x reaches again to ε_c. This process takes place at the disc's displacement and resistance denoted by point M_2. Deactivating the bonding force in the second node brings the resistance to the level indicated by point N_2. Next, this process is repeated. Similarly, there is always a small crack moving in front of the blade that allows the blade to travel through the soil [42]. This separation process is similar to the process of cutting chips in machining operations [43–45].

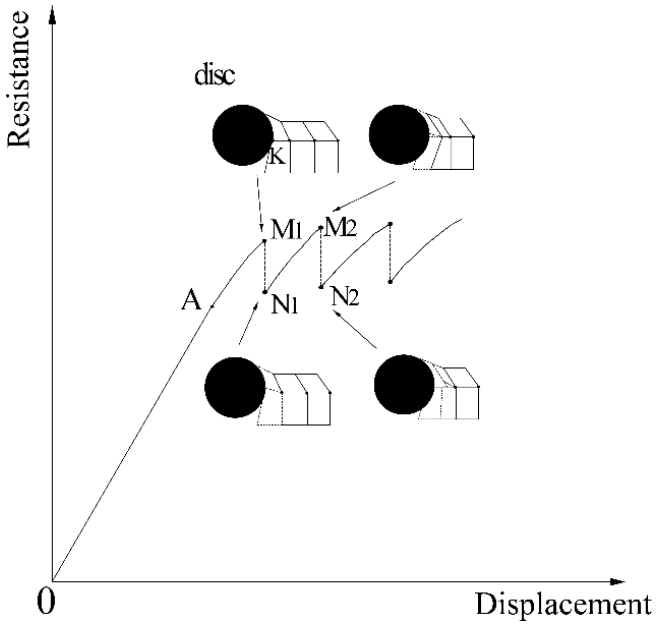

Figure 4. Resistance versus displacement.

The biomimetic disc furrow opener moved at a uniform speed in a fixed direction (i.e., the X direction) and continuously repelled the soil from the furrow for sowing in the numerical simulation. Figure 5 (A–D) shows the four stages of cutting the soil with the biomimetic furrow opener disc. The simulation analysis of the erosion contact requires the contact component (i.e., the biomimetic furrow opener disc) and the target (i.e., the soil) without initial penetration [40]. Therefore, the initial condition of the soil was not in direct contact with the opener disc. The biomimetic disc furrow opener moved in a uniform motion at 1 m/s. The disc furrow opener contacted the soil and then began to compress the soil while continuing to move forward after 0.004 s. The data was collected after the disc opener completely entering the soil model (0.304 s) to reduce the influence on the soil boundary.

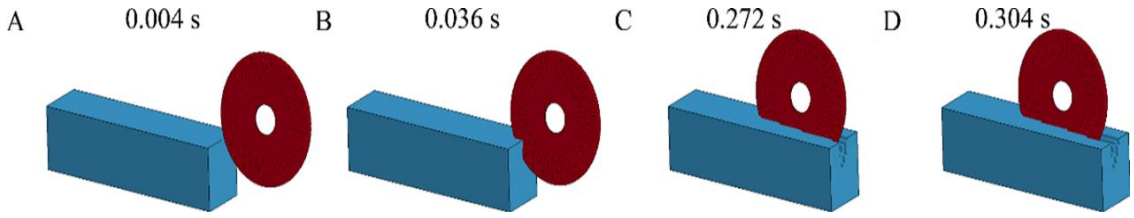

Figure 5. Four stages of soil cutting with the biomimetic disc furrow opener (D-BC-3). (A) The disc has just contact with the soil (0.004 s); (B) the disc enters the soil (0.036 s); (C) the disc just fully enters the soil (0.272 s); (D) the disc runs steadily in the soil (0.304 s).

The resistance of the ordinary disc furrow opener (DISC10) was 159.34 N by the FEM simulation. The resistances of the three types of biomimetic discs with different numbers were shown in Table 5.

From the results in Table 6, it can be observed that the optimum biomimetic structured disc furrow opener is D-BC-3 with minimum resistance (73.81 N, approximately 53.7% less than that of Disc10). (The soil adhesion is ignored in the simulation analysis processing, which leads to the results deviations with the test values).The second one is D-BCH-5 with minimum resistance (77.87 N, approximately 51.1% less than that of Disc10), and the third one is D-BC-54 with minimum resistance (80.22 N, approximately 49.7% less than that of Disc10).The resistances of all three types biomimetic furrow opener discs are less than that of the ordinary disc furrow opener (Disc10). The simulation results showed that biomimetic disc furrow openers reduce resistance and save energy.

The D-BCH-5, D-BC-3 and D-BC-4 discs were manufactured to do tests in soil bin for the performance evaluation.

Table 5. Results for tillage resistance according to simulation analysis (N).

No.	D-BCH	D-BW	D-BC
1	148.97	130.84	131.00
2	90.31	115.17	88.66
3	137.93	102.22	73.81
4	132.07	144.98	80.22
5	77.87	86.70	111.63
6	102.16	121.83	112.19
7	113.45	121.92	96.08
8	102.66	124.85	121.38
9	86.31	86.78	140.91

3.2. Soil bin test results

The horizontal resistance values of D-BCH-5, D-BC-3, D-BC-4 and DISC10 under different conditions (soil moisture content = 15% and 20%, furrow speed = 0.6, 1 and 1.4 m/s) were shown in Figure 6.

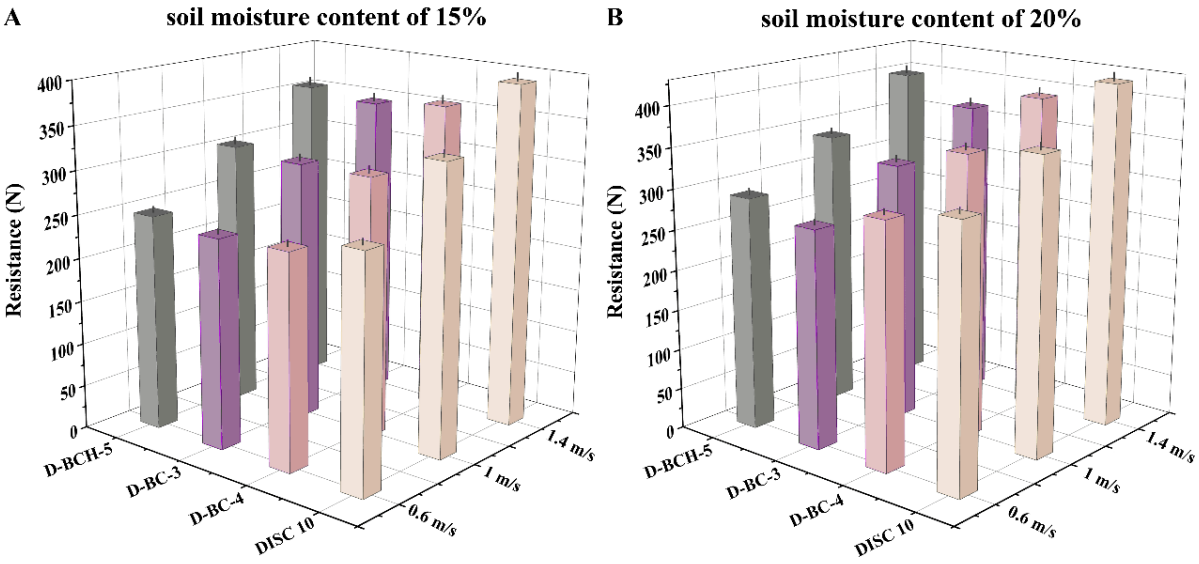

Figure 6. Soil bin resistance test of D-BCH-5, D-BC-3, D-BC-4 and DISC10 under different test conditions. (A) and (B) are soil moisture content of 15% and 20%, respectively.

To compare the resistance-reducing among three biomimetic discs, the resistance-reducing rate β (%) of biomimetic furrow opener discs was evaluated.

$$\beta = \frac{F_{r10} - F_{rb}}{F_{r10}} \tag{9}$$

Where F_{r10} - the resistance of Disc 10, F_{rb} - the resistance of biomimetic disc furrow opener.

Generally, furrow speed and soil moisture content both influenced the furrow resistances significantly. The resistance-reducing rate of biomimetic disc furrow openers obviously outperformed that of Disc 10. The resistance-reducing rate of D-BC-3 reached the maximum value 15.36% with the furrow speed of 0.6 m/s and the soil moisture content of 20%.

With the increase of soil moisture content from 15% to 20%, the furrow resistances of D-BCH-5, D-BC-3, D-BC-4 and DISC10 increased by 16.30%, 11.94%, 22.25% and 20.33% respectively at the speed of 0.6 m/s, by 11.40%, 6.81%, 16.59% and 9.94% respectively at the speed of 1 m/s , and by 11.92%, 5.84%, 10.18% and 7.59% respectively at the speed of 1.4 m/s.

With the increase of soil moisture and furrow speed, the furrow resistances increased considerably. Under different moisture contents, as the furrow speed rose from 0.6 to 1.0 m/s and further to 1.4 m/s, the percentage of furrow resistance increased by no more than 5% in each disc, which indicated the linearity between speed and furrow resistance [11]. The furrow resistance increased with the moisture content under different furrow speeds. However, at high furrow speed (1.4 m/s), the effect of furrow resistance was the least with different soil moisture contents, and the average increase rate was only 9.31%. Because the furrow disc at high speed is under high-speed rotation and the soil partially adhering to the disc is thrown away by the centrifugal force, which made the surface structure less affected by the adhesive soil, resulting in the less furrow resistance.

4. Discussion

4.1. Analysis of the stress

The equivalent stress diagram of the interaction between D-BC-3 and the soil during the furrowing process was shown in Figure 7. It reveals that only a small part of the soil is subjected to increased stress, and the stress of the soil in most areas is generally not influenced by the disc furrow opener. The range of the stress variation is small, which indicated few disturbances to the soil. The disturbed soil is accumulated in front of point *K* on the disc (Figure 3) and swelled up in upward and lateral directions with respect to its original configuration. The deformation patterns of the simulations are agreed with what described in the previous research [46].

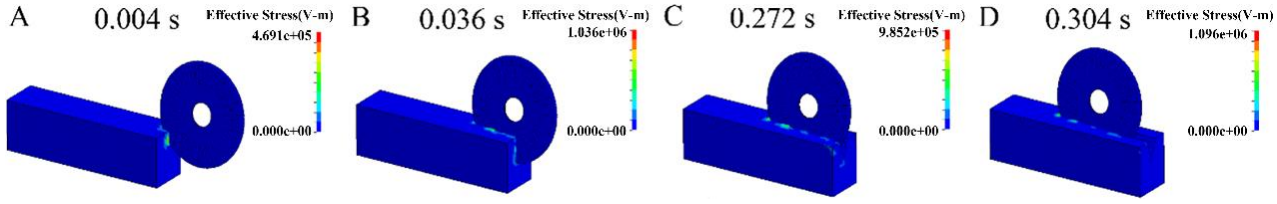

Figure 7. Stress distribution of the biomimetic disc furrow opener (D-BC-3) during the furrowing process.

4.2. Range analysis

The data is analyzed by range analysis, the factors are ordered based on their importance. Range analysis results of the above four factors (h_1, D/L', S_1, δ) are shown in Table 6. It can be seen that D/L', D/L' and δ are the key factors for D-BCH, D-BW and D-BC, respectively. So, it is certainly that surface structures of disc furrow opener affect its work resistance. For the disc furrow opener designed by single biomimetic element (convex hull or wedge), its geometric size has more influence on the resistance than the elements configuration parameter. While for those designed by coupling multiple biomimetic elements (D-BC), the elements configuration parameters have a greater influence on resistance than the geometric size. The influence of each factor on the test of D-BC from high to low was δ, S_1, h_1 and D/L' which provided the meaningful inspirations for optimizing design of drag reduction opener disc.

Table 6. Range analysis results of the four factors.

DISC / factors	D-BCH	D-BW	D-BC
h_1 (mm)	24.93	6.65	21.63
D/L' (mm)	41.22	28.97	6.54
S_1 (mm)	4.13	24.72	34.19
δ (°)	22.5	22.58	36.04

4.3. Analysis of biomimetic structures influence on resistance

The slip resistance of the disc furrow opener is determined by the friction force component [39]. However, under normal and high moisture content conditions, the water film formed by the interface between the soil and furrow opener disc produces a larger interface adsorption force. The larger adsorption force increases the slip resistance of the furrow opener disc, and soil adhered to the disc furrow opener. The morphology of metal surface has an important influence on surface properties [47,48]. The surface of biomimetic disc furrow opener has a biomimetic element structure. The contact between the disc opener and soil is actually a micro-convex contact, which not only makes the actual contact area is smaller than the apparent contact area but affects the contact properties [37]. The convexity formed by these biomimetic elements cause a change in the water film structure between the soil and furrow opener disc interface in this area.

Under the effect of the biomimetic element structure, parts of the single water films break their continuity, and become a number of discontinuous water films [38]. In addition, the thickness b of these newly formed water films increases. When the moisture content is constant, the sum of the area of the newly formed water film is smaller than that of the original one. Then, the total area A of the water film also decreases. According to Eqs. (1), (10) and (11), $F_{s\text{-}a}$ reduces.

And the total absorption load $F_{t\text{-}a}$ produced by the water film can be expressed as follows,

$$F_{t-a} = \Sigma F_{s-a} \tag{10}$$

Therefore, $F_{t\text{-}\alpha}$ produced by the water film decreases with the decrease of $F_{s\text{-}a}$. According to Ahmadi's work [41], in the case of the reduction of $F_{s\text{-}a}$ of the water film and the total water film area, the slip resistance force between the surface of disc furrow opener and the soil also decreases. Then, in the third process, the total slip resistance force of the disc furrow opener produced by the slip between the soil and the disc decreases.

According to the literature [49], the surface contact angle θ can be expressed as follows:

$$\cos\theta = \gamma \cos(\theta_i) \tag{11}$$

Where θ_i - the intrinsic contact angle, γ - the surface roughness.

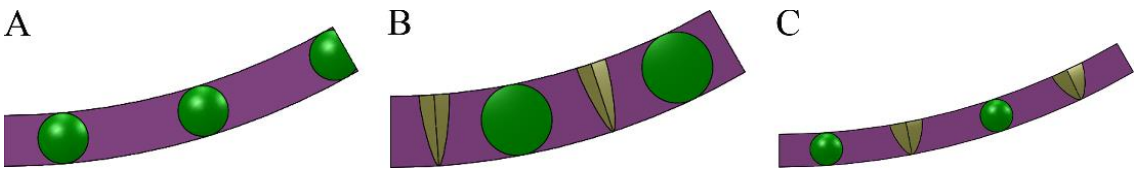

Figure 8. Intercept surfaces of the biomimetic furrow opener disc. A, D-BCH-5; B, D-BC-3; C, D-BC-4.

To investigate their resistance effects, the biomimetic structures of the same ring within 30 degrees of the three biomimetic disc furrow openers are selected for analysis in this paper, as shown in Figure 8. The surface roughness values γ_1, γ_2 and γ_3 are 1.108, 1.067 and 1.191 for D-BCH-5, D-BC-3 and D-BC-4, respectively, namely, $\gamma_3 > \gamma_1 > \gamma_2$. According to Eqs. (10) and (11), the size relation of

F_{w1}, F_{w2} and F_{w3} corresponds to the absorption loads of D-BCH-5, D-BC-3 and D-BC-4, respectively, namely, $F_{w2} < F_{w1} < F_{w3}$. Therefore, the resistance of D-BC-3 is the least in the furrowing process, which is consistent with the result of simulation analysis.

4.4. Analysis of moisture content influence on resistance

Soil adhesion on the disc furrow opener is directly affected by the soil moisture content [50]. When the soil moisture content is low, the soil particles surface only produces adsorption water, namely, the contact between the soil particles micro convex and the metal non-smooth surface only occurs at convex peak area. The interface between soil and furrow opener disc cannot form a water film, resulting in the soil not to adhere to metal surface, as shown in Figure 9A.

With the increase of moisture content, the water film on micro convex surface increases. When the thickness of water film is larger than the distance that between micro convex and metal surface, the state transforms from completely non-contact to liquid point contact, and which increases adhesion gradually [17], as shown in Figure 9B. At the same time, water tension decreases with increasing of moisture content. However, it will produce a better continuous water film with more unity thickness, which increases the actual contact area between metal and soil. The trend of area increasing is more than that of water intension decreasing. Then, the adhesion will increase to the maximum.

When the interface between soil particles and metal surface produces independent water ring, there will be interactions between soil, water and metal surface, as shown in Figure 9C. The water ring extends downward from the top of contact peak, forming water film, as shown in Figure 1. Because the interface of water film is affected by soil and metal two force fields, the energy distribution on water film will be changed. The closer to the interface, the higher the interaction potential of interface, results in lower energy of water film [51]. However, a high-energy surface occurs in the middle of water film, where the energy is higher than adjacent water. The weakest area of interface between soil and metal is the sum of high-energy surfaces in the contact water film. The total high-energy area is the actual contact area between the soil and metal surface. Water film thickness increases with increasing moisture content. Eventually, the contact surface will be completely separated by a thicker film of water [52]. According to Eqs. (9) and (10), $F_{s\text{-}a}$ will be weakened.

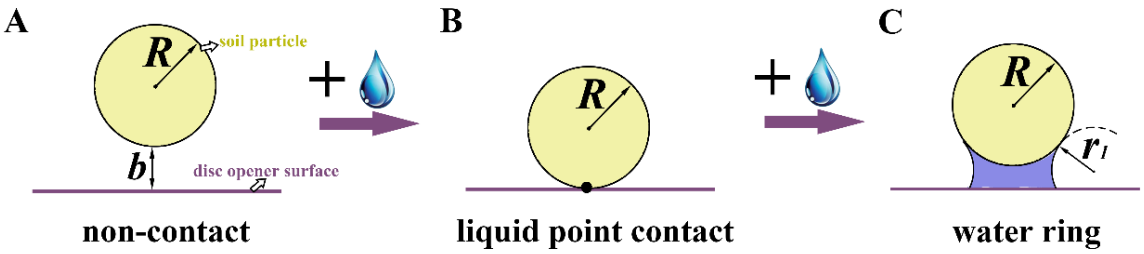

Figure 9. Interface between metal and soil with increasing of moisture content. A, non-contact; B, liquid point contact; C, independent water ring. R-the radius of soil particle.

In this paper, the furrow resistances of disc openers increase with the increase of soil moisture content from 15% to 20%. It indicated that this moisture content interval corresponded to the processing B to C. Future work can increase this range to discuss the moisture content at the time of maximum adhesion.

4.5. Analysis of furrow speeds influence on resistance

It is assumed that disc opener moves forward at a constant velocity v, that is, the soil moves backward with v. At this point, the tangential soil adhesion on the disc opener will produce tangential resistance Fat [32], as shown in Eq. (12).

$$F_a^t = 4\pi Rr\cos\theta \tag{12}$$

When the relative sliding occurs on the interface between disc opener and soil, the soil meniscus will deform, as shown in Figure 10. It indicates that the static contact angle θ in front of the soil movement becomes advancing contact angle θ_1. And the static contact angle θ in back of the soil movement becomes receding contact angle θ_2. Where $\theta_1 > \theta > \theta_2$. Obviously, the horizontal component of interface tension F_2 plays a role in hindering soil movement. Corresponding, the horizontal component of interface tension F_1 acts as an impediment to movement of disc opener.

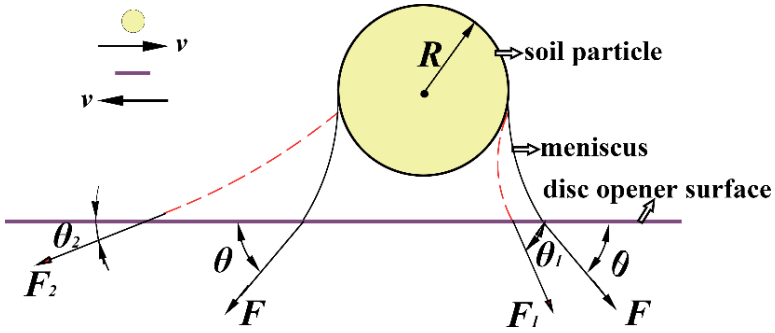

Figure 10. Schematic diagram of tangential resistance f meniscus. v – velocity; θ – static contact angle; θ1 – advancing contact angle; θ2 – receding contact angle; F, F1, F2 – interface tension.

If $F_1 = F_2 = F$, according to Eq. (11), the formula for quantitative analysis of tangential resistance F_a^t', namely, combined force of horizontal components, is shown in Eq. (13).

$$F_a^t{}' = Fl(\cos\theta_2 - \cos\theta_1) \tag{13}$$

Where l – action length of F_1 and F_2 (assuming they are equal).

F_a^t' is affected by θ_1 and θ_2, which forms by changing in the movement of soil-disc opener interface system. The variation of θ_1 and θ_2 is related with the furrow speed and the disc opener surface structure. θ_1 will become obtuse angle and θ_2 tends to 0 with a higher velocity, which increases F_a^t', that is, increasing adhesion [53]. Figure 6 shows that the furrow resistance increases with the increase of furrow speed, which is consistent with the theory analysis.

5. Conclusion

In this paper, resistance-reducing mechanism of biomimetic furrow opener disc was investigated for reducing effect of furrowing resistance and soil adhesion. Based on the biomimetic design principles, the convex hull of the dung beetle's pronotum and the wedge in dorsal scales of the pangolin

were selected as the bionic prototypes for obtaining the biomimetic disc furrow opener, and optimized the disc opener design to reduce furrow resistance and improve energy efficiency by FEM. In following, test verification was performed in the soil bin, and the soil-disc interaction, analysis of the different factors influence on resistance and the effect of soil disturbance were discussed.

Water film state played a major role in soil-metal adhesion, which depended on area, shape, and distribution (contact point continuity and uniformity) of contact point. So, changing the metal surface structures can cause a change in the water film structure between soil and metal interface.

Biomimetic convex hull structure (D-BCH), biomimetic wedge structure (D-BW) and biomimetic coupled structure with convex hull and wedge (D-BC) were performed on the ordinary disc using the orthogonal test design technique. The simulation results showed that biomimetic disc furrow openers reduced resistance and saved energy. The optimum biomimetic structured disc furrow opener was D-BC-3, the one with minimum resistance (73.81 N; approximately 53.7% less than that of Disc10), which had the following configuration: δ=7.2°, S_1=6 mm, h_1=1 mm and D/L'=14 mm.

Range analysis results of the four factors (h_1, D/L', S_1, δ) showed that D/L', D/L' and δ were the key factors for D-BCH, D-BW and D-BC, respectively. The influence of each factor on the test of D-BC from high to low was δ, S_1, h_1 and D/L'. It was of great significance for the future design of drag reduction disc opener.

The equivalent stress diagram of the interaction between D-BC-3 and the soil revealed that only a small part of the soil was subjected to increased stress, and the stress of the soil in most areas was generally not influenced by the disc furrow opener. The range of the stress variation was small, which indicated few disturbances to the soil.

According to simulation results, D-BCH-5, D-BC-3 and D-BC-4 discs were chosen to do test in soil bin with two different soil moisture contents of 15% and 20%, and three furrow speeds of 0.6, 1 and 1.4 m/s. The test results showed that the resistance of the biomimetic disc furrow opener was less than that of the ordinary disc due to the biomimetic disc's reduced absorption force and slip resistance. The resistance-reducing rate of D-BC-3 reached the maximum value 15.36%at the furrow speed of 0.6 m/s and the soil moisture content of 20%. With the increase of soil moisture and furrow speed, the furrow resistance of furrow disc increased considerably. As the soil moisture content increased from 15% to 20%, the furrow resistances of D-BCH-5, D-BC-3, D-BC-4 and DISC10 increased from 5.84% to 22.25%.

The surface roughness of D-BC-3 was less than that of D-BCH-5 and D-BC-4, resulted in the least resistance, which agreed with the simulation results.

A better continuous water film with more unity thickness were produced with the increase of moisture content, resulted in the increasing of actual contact area, which was more than that of water intension decreasing. Soil moisture content interval from 15% to 20% corresponded the processing from liquid point contact to independent water ring. Future work can increase this range to discuss the moisture content at the time of maximum adhesion.

Tangential resistance of interface tension $F_a{}^{t}{}'$ was affected by advancing contact angle θ_1 and receding contact angle θ_2, which formed by changing in the movement of soil-disc opener interface system. θ_1 became obtuse angle and θ_2 tended to 0 with a higher velocity, which increased $F_a{}^{t}{}'$, that is, increasing adhesion. The furrow resistance increased with the increase of furrow speed, which was consistent with the theory analysis.

It should be further researched and explored in the subsequent design of biomimetic opener disc with the influence of two biomimetic coupling elements on the change of furrow resistance under the

condition of uneven distribution on the disc and the orientation of wedge shape.

Acknowledgments

This work was supported by National Key R&D Program of China (No. 2016YFE0112100), the China-EU H2020 FabSurfWAR Project (No. 644971), and the 111 project (No. B16020) of China, and the China Scholarship Council, China (CSC).

Conflict of interest

All authors declare no conflicts of interest in this paper.

References

1. D. P. Darmora, K. P. Pandey, Evaluation of performance of furrow openers of combined seed and fertiliser drills, *Soil Till. Res.*, **34** (1995), 127–139.
2. C. Sawant, A. Kumar, I. Mani, J. K. Singh, Soil bin studies on the selection of furrow opener for conservation agriculture, *J. Soil Water Conserv.*, **15** (2016), 107–112.
3. P. Y. Guo, M. A. Choudhary, Preliminary studies of a modified slot opener for direct drilling seeds, *New Zeal. J. Exp. Agric.*, **1** (1985), 85–95.
4. A. Bahri, R. K. Bansal, Evaluation of different combination of furrow openers and press wheels for no till seeding, *Homme. Terre. Eaux.*, **22** (1992), 55–66.
5. A. Ozmerzi, Seed distribution performance of furrow openers used on drill machines, *AMA-Agr. Mech. Asia AF.*, **17** (1986), 32–34.
6. F. Ahmad, D. Weimin, D. Qishuo, M. Hussain, K. Jabran, Forces and straw cutting performance of double disc furrow opener in no-till paddy soil, *PLoS One*, **10** (2015), e0119648.
7. T. Vamerali, M. Bertocco, L. Sartori, Effects of a new wide-sweep opener for no-till planter on seed zone properties and root establishment in maize (*Zea mays*, L.): A comparison with double-disk opener, *Soil Till. Res.*, **89** (2006), 196–209.
8. A. A. Tagar, C. Ji, J. Adamowski, J. Malard, C. S. Qi, Q. S. Ding, N. A. Abbasi, Finite element simulation of soil failure patterns under soil bin and fieldtesting conditions, *Soil Till. Res.*, **145** (2015), 157–170.
9. H. A. Nidal, C. R. Randall, A nonlinear 3D finite element analysis of the soil forces acting on a disk plow, *Soil Till. Res.*, **74** (2003), 115–124.
10. H. Bentaher, A. Ibrahmi, E. Hamza, M. Hbaieb, G. Kantchev, A. Maalej, W. Arnold, Finite element simulation of moldboard–soil interaction, *Soil Till. Res.*, **134** (2013), 11–16.
11. B. A. Collins, D. B. Fowler, Effect of soil characteristics, seeding depth, operating speed, and opener design on draft force during direct seeding, *Soil Till. Res.*, **39** (1996), 199–211.
12. S. Q. Zhang, X. Ma, C. C. Zuo, C. L. Ma, H. W. Wang, Y. J. Sun, Forces acting on disk colter and computer simulation, *Trans. CSAE.*, **11** (1995), 52–56.
13. S. Q. Zhang, C. C. Zuo, C. L. Ma, The study on the model of disc coulter force, *Trans. CSAM*, **29** (1998), 71–75.
14. J. L. Jiang, L. N. Gong, M. F. Wang, Study on the working performance of the no-tillage planter unit, *Trans. CSAE*, **16** (2000), 64–66.

15. E. M. Tice, J. G. Hendricks, Disc coulter forces: evaluation of mathematical models, *Trans. ASAE*, **34** (1991), 2291–2298.
16. J. Tong, B. Z. Moayad, Y. H. Ma, J. Y. Sun, D. H. Chen, H. L. Jia, L. Q. Ren, Effects of biomimetic surface designs on furrow opener performance, *J. Bionic. Eng.*, **6** (2009), 280–289.
17. L.Q. Ren, Progress in the bionic study on anti-adhesion and resistance-reducing of terrain machines, *Sci. China Ser. E.*, **52** (2009), 273–284.
18. L. Q. Ren, D. X. Chen, J. G. Hu, Preliminary analysis on the rules of decreasing viscosity and removing rabbits of soil animals, *J. Agr. Eng.*, **6** (1993), 15–20.
19. B. C. Cheng, L. Q. Ren, X. B. Xu, Bionic study on soil adhesion (two) A preliminary study on the anti-viscosity and desorption of the body surface of typical soil animals, *J. Agr. Eng.*, **6** (1990), 2–6.
20. L. Q. Ren, *Experimental Design and Optimization*, Science Press, (2009).
21. D. W. Bechert, M. Bruse, W. Hage, J. G. T. van der Hoeven, G. Hoppe, Experimentson drag reducing surfaces and their optimization with an adjustable geometry, *J. Fluid Mech.*, **338** (1997), 59–87.
22. J. B. Zhang, J. Tong, Y. H. Ma, Abrasive wear characteristics of subsoiler tines with bionic rib structure surface, *Jilin Daxue Xuebao (Gongxueban)*,**45** (2015), 174–180.
23. Z. J. Zhang, H. L. Jia, J. Y. Sun, Abrasive wear characteristics of subsoiler tines with bionic rib structure surface, *Adv. Mech. Eng.*, **7** (2015), 1–11.
24. V. Zorba, E. Stratakis, M. Barberoglou, E. Spanakis, C. Fotakis, Biomimetic artificial surfaces quantitatively reproduce the water repellency of a lotus leaf, *Adv. Mater.*, **20** (2008), 4049–4054.
25. H. Lee, B. P. Lee, P. B. Messersmith, A reversible wet/dry adhesive inspired by mussels and geckos, *Nature*, **448**(2007), 338–341.
26. X. Li, T. Chen, Enhancement and suppression effects of a nanopatterned surface on bacterial adhesion, *Phys. Rev. E*, **93**(2016), 52419.
27. D. C. Zeng, *Mechanical Soil Dynamics*, Beijing Science and Technology Press, (1995).
28. L. D. Bevel, W. H. Gardner, W. R. Gardner, *Soil Physics*, John Wiley & Sons., (1956).
29. P. G. Huray, *Maxwell's Equations*, Wiley-IEEE Press, (2009).
30. D. H. Qian, J. X. Zhang, A summary of study of adhesion and friction between soil and metals, *Trans. CSAM*, **1** (1984), 71–80.
31. D. H. Qian, A summary of study of adhesion and friction between soil and metals, *Trans. CSAM*, **2** (1965), 47–52.
32. L. Q. Ren, *Soil Adhesion Mechanics*, China Machine Press, (2011).
33. R. E. Baier, E. G. Shafrin, W. A. Zisman, Adhesion: mechanisms that assist or impede it, *Science*, **162** (1968), 1360–1368.
34. R. A. Fisher, Further note on the capillary forces in an ideal soil, *J. Agr. Sci.*, **18** (1928), 406–410.
35. M. L. Nichols, The sliding of metal over soil, *Agric. Eng.*, **6** (1925), 80–84.
36. W. B. Haines, Studies in the physical properties of soils: I. Mechanical properties concerned in cultivation, *J. Agr. Sci.*, **15** (1925), 178–200.
37. S. Q. Deng, L. Q. Ren, Y. Liu, Z. W. Han, Tangent resistance of soil on moldboard and the mechanism of resistance reduction of bionic moldboard, *J. Bionic Eng.*, **2** (2005), 33–46.
38. L. Q. Ren, J. Tong, J. Q. Li, B. C. Chen, Soil adhesion and biomimetics of soil-engaging components: a review, *J. Agr. Eng. Res.*, **79** (2001), 239–263.
39. W. R. Gill, C. E. Vandenberg, *Soil Dynamics in Tillage and Traction*, Chinese Agricultural

Machinery Press, (1983).
40. B. A. Lewis, Manual for LS-DYNA Soil Material Model 147, Federal Highway Administration, (2004).
41. I. Ahmadi, Development and assessment of a draft force calculator for disk plow using the laws of classical mechanics, *Soil Till. Res.*,**163** (2016), 32–40.
42. A. Armin, R. Fotouhin, W. Szyszkowski, On the FE modeling of soil–blade interaction in tillage operations, *Finite Elem. Anal. Des.*, **92** (2014), 1–11.
43. N. Eu-Gene, D. K. Aspinwall, Modeling of hard part machining, *J. Mater. Process. Tech.*, **127** (2002), 222–229.
44. J. M. Huang, J. T. Black, An evaluation of chip separation criteria for the fem simulation of machining, *J. Manuf. Sci. Eng.*, **118** (1996), 461–469.
45. A. P. Markopoulos, *Finite Element Method in Machining Process*, Springer, (2013).
46. A. Z. Shmulevich, D. Rubinstein, Interaction between soil and a wide cutting blade using the discrete element method, *Soil Till. Res.*, **97** (2007), 37–50.
47. D. L. Jing, S. K. Yi, Electroosmotic flow in tree-like branching microchannel network, *Fractals*, **27** (2019), 1950095.
48. D. L. Jing, J. Song, Y. Sui, Hydraulic and thermal performances of laminar flow in fractal treelike branching microchannel network with wall velocity slip, *Fractals*, **28** (2020), 2050022.
49. X. Jia, Unsmooth cuticles of soil animals and theoretical analysis of their hydrophobicity and anti-soil-adhesion mechanism, *J. Colloid Inter. Sci.*, **295** (2006), 490–494.
50. E. R. Fountaine, Investigations into the mechanism of soil adhesion, *J. Soil Sci.*, **5** (1954), 251–263.
51. F. M. Fowkes, Additivity of intermolecular forces at interfaces. I determination of the contribution to surface and interfacial tensions of dispersion forces in various liquids, *J. Phys. C*, **67** (1963), 2538–2541.
52. I. Lifshitz, The kinetics of precipitation from supersaturated solid solutions, *J. Phys. Chem. Solid*, **19** (1961), 35–50
53. J. Bachmann, A. Ellies, K.H. Hartgea, Development and application of a new sessile drop contact angle method to assess soil water repellency, *J. Hydrol.*, **231–232** (2000), 66–75.

AIMS Press